Curvature and Hydrophobic Forces Drive Oligomerization and Modulate Activity of Rhodopsin in Membranes

Ana Vitória Botelho,* Thomas Huber,† Thomas P. Sakmar,† and Michael F. Brown*‡§
*Department of Biochemistry and Molecular Biophysics, ‡Department of Chemistry, and §Department of Physics, University of Arizona, Tucson, Arizona; and †Laboratory of Molecular Biology and Biochemistry, The Rockefeller University, New York, New York

ABSTRACT G protein-coupled receptors (GPCRs) are essential components of cellular signaling pathways. They are the targets of many current pharmaceuticals and are postulated to dimerize or oligomerize in cellular membranes in conjunction with their functional mechanisms. We demonstrate using fluorescence resonance energy transfer how association of rhodopsin occurs by long-range lipid-protein interactions due to geometrical forces, yielding greater receptor crowding. Constitutive association of rhodopsin is promoted by a reduction in membrane thickness (hydrophobic mismatch), but also by an increase in protein/lipid molar ratio, showing the importance of interactions extending well beyond a single annulus of boundary lipids. The fluorescence data correlate with the pK_a for the MI-to-MII transition of rhodopsin, where deprotonation of the retinylidene Schiff base occurs in conjunction with helical movements leading to activation of the photoreceptor. A more dispersed membrane environment optimizes formation of the MII conformation that results in visual function. A flexible surface model explains both the dispersal and activation of rhodopsin in terms of bilayer curvature deformation (strain) and hydrophobic solvation energy. The bilayer stress is related to the lateral pressure profile in terms of the spontaneous curvature and associated bending rigidity. Transduction of the strain energy (frustration) of the bilayer drives protein oligomerization and conformational changes in a coupled manner. Our findings illuminate the physical principles of membrane protein association due to chemically nonspecific interactions in fluid lipid bilayers. Moreover, they yield a conceptual framework for understanding how the tightly regulated lipid compositions of cellular membranes influence their protein-mediated functions.

INTRODUCTION

As the receptors for biogenic amines, chemokines, odorants, and light, G protein-coupled receptors (GPCRs) have attracted intense interest (1,2). GPCRs such as rhodopsin (3,4) comprise $>10^3$ members in the human genome (1). Apart from their biological roles as sensors of hormonal, neuronal, and chemotactic signals, they are the targets of about 50% of the pharmaceuticals used worldwide (5). One topic that has stimulated considerable attention is the oligomeric state of GPCRs in connection with biological signaling (1,5–8). Association of GPCRs in cellular membranes has far-reaching implications for understanding signal transduction (1), drug discovery (1,5), neuroscience (6), and immunology (9). A related aspect is that receptor association in cellular membranes may involve lipid rafts, originally conceived as functional microdomains. In the fluid-mosaic model the lipid bilayer acts as an inert 2D solvent, whereas the raft hypothesis states that interactions of signaling proteins occur within lipid regions on the cell surface (10,11). Attempts have been made to correlate seven-helical receptor association with function, yet significant controversy remains concerning the functional relevance of receptor oligomerization and the role of membrane lipids in this process. For rhodopsin (3,4,12–14), in particular, the issue of oligomerization has emerged as a topic of intense discussion (2,7).

In this article, we describe studies of the canonical GPCR rhodopsin that entail a well-defined membrane system whose compositional variables are precisely controlled. Rhodopsin, the dim light photoreceptor, is the only family A GPCR for which a 3D crystal structure is currently available (13,15). In the dark state, the retinylidene cofactor is in a highly distorted configuration that is implicated with its ultrafast photochemistry (16). Absorption of a photon initiates 11-*cis* to *trans* isomerization of the chromophore, followed by a series of thermal relaxations (17–19) culminating in an equilibrium between two forms, MI and MII, leading to phototransduction. In the activated MII conformation, the retinylidene Schiff base is deprotonated, thus disrupting the salt bridge to the carboxylate of Glu^{113}, the counterion (3,4,12). The resulting conformational change may reposition the β-ionone ring (20,21), which together with helical movements (4,21) exposes previously hidden recognition sites for the cognate G protein (3,4). Activation of G_t (transducin) is followed by further amplification through a phosphodiesterase effector (3) yielding visual perception. An important question is the role of the membrane lipid composition in the activation of rhodopsin and downstream visual signaling (22).

Now, in studies of GPCR oligomerization in cellular membranes (6,9), as well as proteins in lipid rafts, fluorescence resonance energy transfer (FRET) has emerged in a pivotal role (10,23). FRET studies of fluorescent protein-tagged GPCRs in native cellular membranes have provided

Submitted February 7, 2006, and accepted for publication September 19, 2006.

Ana Vitória Botelho and Thomas Huber contributed equally to this work.

Address reprint requests to Michael F. Brown, Dept. of Chemistry, University of Arizona, Tucson, AZ 85721. Tel.: 520-621-2163; Fax: 520-621-8407; E-mail: mfbrown@u.arizona.edu.

0006-3495/06/12/4464/14 $2.00

doi: 10.1529/biophysj.106.082776

evidence for significant receptor association in living cells (6). Yet for glycosylphosphatidylinositol (GPI)-linked proteins, FRET microscopy indicates a random (ideal) distribution, a finding that is seemingly incompatible with protein clustering in lipid rafts (23). What is lacking, however, are investigations of well-defined membrane systems where lipid-protein interactions can be distinguished from protein-protein interactions, e.g., as seen in the crystal structure of rhodopsin (13,15). Our research has monitored constitutive association of rhodopsin through FRET investigations of the visual receptor labeled with site-specific fluorophores. We discovered systematic changes in association of rhodopsin in the dark state due to the membrane lipid composition, similar to the results from earlier work (24,25). Moreover, nonrandom mixing of rhodopsin was inversely correlated with its photoactivation, suggesting a link to visual signal transduction. Both association and photoactivation of rhodopsin were strongly influenced by the protein packing density within the membrane, as well as hydrophobic matching, showing the effect of crowding of the receptors. Influences of rhodopsin-lipid interactions on protein association and activity are described by the spontaneous (intrinsic) curvature of the fluid membrane (26) in terms of a simple flexible surface model (FSM) (27). Several preliminary accounts of this work have appeared (28–30).

MATERIALS AND METHODS

Preparation of recombinant membranes

Native rod membranes were isolated from frozen bovine retinas as described in previous work (31). Purification of rhodopsin was carried out using a 1D4 anti-rhodopsin antibody. Rhodopsin was eluted 4 × with 1 mL of buffer (25 mM MES, 25 mM K HEPES, 125 mM KCl, 1 mM EDTA, pH 6.7) containing 1.5% (w/v) β-octylglucoside (OG) and 0.36 mg/mL of the C-terminal rhodopsin nonapeptide per mL of gel, giving $A_{280}/A_{500} = 1.6$–1.7. Rhodopsin plus the appropriate phospholipids (Avanti Polar Lipids, Alabaster, AL) were solubilized with 1.5% OG plus 1.5% (w/v) sodium cholate (32) and recombined by dialysis against buffer. All membrane samples gave a single predominant band with isopycnic sucrose density gradient centrifugation whose position depended on the protein/lipid molar ratio (not shown).

Fluorescence measurements

Rhodopsin in rod disk membranes was labeled at position Cys^{316} with the donor Alexa Fluor 488 C_5 maleimide or the acceptor Alexa Fluor 594 C_5 maleimide (Invitrogen, Carlsbad, CA). Purified proteins were mixed in equal stoichiometry and incorporated into recombinant membranes. Measurements were performed at 20°C using a SPEX-Fluorolog τ3 spectrofluorometer (Horiba Jobin Yvon; Edison, NJ) fitted with excitation and emission single-grating monochromators. The fluorescence signal $F^{\mathrm{em}}_{\mathrm{exc}}$ depends on the excitation and emission wavelengths of the donor only (D), the acceptor only (A), or both together (DA). Emission of the Rho-Alexa 594 acceptor was used to calculate the energy transfer efficiency E (33) according to:

$$E = \left\{\frac{F^{\mathrm{A}}_{\mathrm{D}}(DA)}{F^{\mathrm{A}}_{\mathrm{A}}(DA)} - \left[\frac{F^{\mathrm{D}}_{\mathrm{D}}(DA)}{F^{\mathrm{A}}_{\mathrm{A}}(DA)}\right]\left[\frac{F^{\mathrm{A}}_{\mathrm{D}}(D)}{F^{\mathrm{D}}_{\mathrm{D}}(D)}\right] - \frac{F^{\mathrm{A}}_{\mathrm{D}}(A)}{F^{\mathrm{A}}_{\mathrm{A}}(A)}\right\}\left(\frac{A_{\mathrm{A}}}{A_{\mathrm{D}}}\right). \quad (1)$$

Here, $F^{\mathrm{A}}_{\mathrm{A}}$ indicates the acceptor excited at 590 nm with emission at 620 nm; $F^{\mathrm{D}}_{\mathrm{D}}$ is the signal of the donor with excitation at 485 nm and emission at 515 nm; and $F^{\mathrm{A}}_{\mathrm{D}}$ refers to donor excitation at 485 nm and acceptor emission at 620 nm. The factor $A_{\mathrm{A}}/A_{\mathrm{D}} = \varepsilon^{\mathrm{A}}_{590}/\varepsilon^{\mathrm{D}}_{485}$ denotes the acceptor/donor absorption ratio. Fluorescence signals from DA pairs were measured for rhodopsin/phospholipid vesicles; whereas individual D and A intensities were for rhodopsin/OG micelles.

Analysis of pH-dependent photoproducts

UV-visible measurements were conducted at 20°C with a Lambda 19 spectrophotometer (PerkinElmer, Wellesley, MA) having an attachment for highly scattering samples, with a total acquisition time of 39 s per spectrum (slit width 2 nm). Equilibrium of the photoproducts was probed by rapid pH adjustment after photolysis of samples containing CCCP (carbonyl cyanide *m*-chlorophenylhydrazone) and valinomycin. The fraction of rhodopsin bleached (f) was calculated using: $f = \Delta A^{\mathrm{d-h}}_{500}/\Delta A^{\mathrm{d-h}}_{500}$, where $\Delta A^{\mathrm{d-h}}_{500}$ is the dark minus light+hydroxylamine absorption difference at 500 nm, and $\Delta A^{\mathrm{d-h}}_{500}$ is the dark minus fully bleached difference at 500 nm. Typically, 89 ± 7% of rhodopsin was photolyzed by the actinic light. The fraction of photoproducts having a deprotonated Schiff base (θ) was calculated using: $\theta = [(\Delta A^{\mathrm{l-d}}_{390} - \Delta A^{\mathrm{l-d}}_{426})/\Delta\varepsilon^{\mathrm{MII-MI}}_{390}]/\Delta A^{\mathrm{d-h}}_{500}/\varepsilon^{\mathrm{Rho}}_{500} + \Delta\varepsilon^{\mathrm{Rho-MI}}_{390}/\Delta\varepsilon^{\mathrm{MII-MI}}_{390}$. Here, $\Delta A^{\mathrm{l-d}}_{390}$ is the light minus dark absorption difference at 390 nm and $\Delta A^{\mathrm{l-d}}_{426}$ is the light minus dark difference at the isosbestic point of 426 nm, which corrects for light scattering changes; $\Delta\varepsilon^{\mathrm{Rho-MII}}_{390} = 34{,}800\ \mathrm{M^{-1}\,cm^{-1}}$ and $\Delta\varepsilon^{\mathrm{Rho-MI}}_{390} = -7200\ \mathrm{M^{-1}\,cm^{-1}}$, yielding $\Delta\varepsilon^{\mathrm{MII-MI}}_{390} = 42{,}000\ \mathrm{M^{-1}\,cm^{-1}}$. UV-visible pH titration curves were fit to three independent pK_{a} values (pK_{a1}, pK_{a2}, and pK_{a3}) using the formula

$$\theta = \frac{10^{\mathrm{pK_{a2}-pH}} + 10^{\mathrm{pH-pK_{a3}}}}{1 + (1 + 10^{\mathrm{pK_{a1}-pH}})10^{\mathrm{pK_{a2}-pH}} + 10^{\mathrm{pH-pK_{a3}}}}. \quad (2)$$

The equilibrium constants for the individual steps are $K_1 = 10^{(\mathrm{pH-pK_{a1}})}$, $K_2 = 10^{(\mathrm{pH-pK_{a2}})}$, and $K_3 = 10^{(\mathrm{pH-pK_{a3}})}$. For the pH 6–8 range, inverted bell-shaped pH titration curves were obtained; assuming that p$K_{\mathrm{a1}} \ll$ pH, the term containing pK_{a1} vanished. The remaining free parameters were pK_{a2} and pK_{a3}; the latter was varied or frozen at 7.8.

RESULTS

Lipid-driven association and dispersal of rhodopsin in membranes

FRET has been previously used to study rhodopsin interactions (32–34), as well as interactions of rhodopsin with transducin (35). For the FRET experiments, we labeled rhodopsin (Rho) at Cys^{316} either with the donor Alexa 488 (Fig. 1 *a*) or acceptor Alexa 594 (Fig. 1 *b*) maleimides (cf. Supplementary Material). All experiments were carried out in the dark state of rhodopsin at 20°C. Due to overlap of the absorption spectrum of rhodopsin in the dark state with the emission spectrum of Alexa 488, quenching of the donor fluorescence emission by the retinal chromophore can occur as an additional decay channel (32,33). For this reason, the FRET experiments were conducted at a very low light intensity to minimize bleaching of rhodopsin. Fluorescence excitation and emission spectra of rhodopsin conjugates in octylglucoside (OG) micelles were intense and well differentiated, with appreciable spectral overlap (Fig. 1 *c*). Control experiments (Fig. 1 *d*) substantiated the absence of significant FRET for rhodopsin in nonionic detergent micelles, where it is monomeric (2,33). Cross-talk of the Alexa 488 donor emission

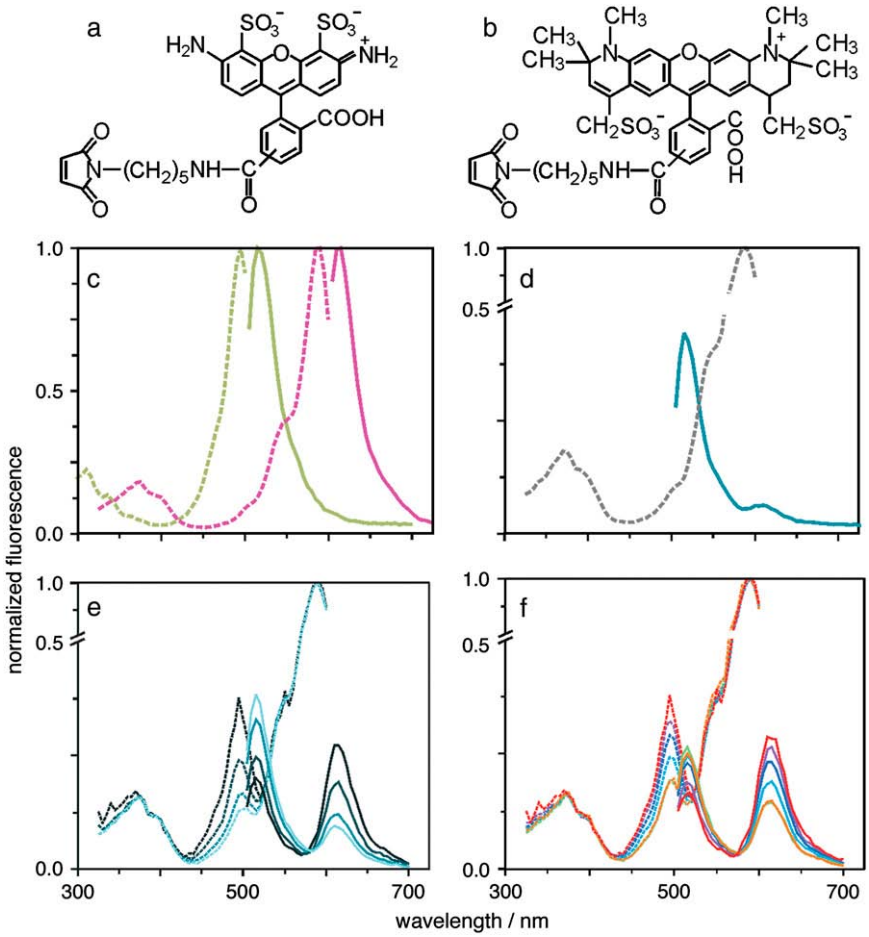

FIGURE 1 FRET measurements reveal association of rhodopsin in recombinant membranes of defined composition. (*a* and *b*) Structures of (*a*) Alexa 488 C_5-maleimide (donor) and (*b*) Alexa 594 C_5-maleimide (acceptor) used to label rhodopsin. (*c*) Normalized excitation spectra (*dotted lines*) and emission spectra (*solid lines*) of Rho-Alexa 488 ($\lambda_{exc} = 495$ nm, $\lambda_{em} = 515$ nm (*green lines*)) and Rho-Alexa 594 ($\lambda_{exc} = 595$ nm, $\lambda_{em} = 620$ nm (*purple lines*)) conjugates recorded separately in 1.5% OG at pH 6.7. (*d*) Control excitation spectra ($\lambda_{em} = 620$ nm (*dotted gray lines*)) and emission spectra ($\lambda_{exc} = 485$ nm (*solid blue lines*)) of 1:1 mixture of Rho-Alexa 488 and Rho-Alexa 594 in 1.5% OG at pH 6.7. Bottom two panels show fluorescence excitation spectra ($\lambda_{em} = 620$ nm (*dotted lines*)) and emission spectra ($\lambda_{exc} = 485$ nm (*solid lines*)) for 1:1 Rho-Alexa 488 and Rho-Alexa 594 pairs in the dark state at pH 6.7 and 20°C. (*e*) Rhodopsin in POPC membranes with protein/lipid ratios (*P*/*L*) of 1:50 (*black lines*), 1:100 (*dark blue lines*), 1:200 (*blue lines*), and 1:400 (*light blue lines*) (descending order at 620 nm). (*f*) Rhodopsin in di(*n*:1)PC membranes with $n = 24$ (*red lines*), 14 (*purple lines*), 16 (*deep blue lines*), 18 (*blue lines*), 22 (*orange lines*), and 20 (*green lines*) acyl carbons, with *P*/*L* = 1:100 (descending order at 620 nm); exact lipids are given in Supplementary Material. All protein/lipid ratios are within ±10%. Intensities are normalized to excitation of Rho-Alexa 594 at 590 nm.

with the acceptor Alexa 594 is very small or negligible and vice versa.

Most intriguing, we discovered systematic changes in FRET as the membrane lipid composition was varied. Rhodopsin was reconstituted in membrane lipid bilayers using a high-throughput approach (cf. Supplementary Material). First, we obtained fluorescence excitation and emission spectra for equimolar Rho-Alexa 488 and Rho-Alexa 594 pairs recombined with 1-palmitoyl-2-oleoyl-*sn*-glycero-3-phosphocholine (POPC) with stoichiometric protein/lipid molar ratios, viz., different protein packing densities. Fig. 1 *e* shows that a decrease in the protein/lipid ratio from 1:50 to 1:400 gave a progressive loss of donor excitation intensity at 485 nm and a gain in emission at 515 nm, together with a reduction of acceptor emission at 620 nm. Greater dispersal of rhodopsin within the bilayer gave a dramatic loss of FRET, as expected due to an increased donor-acceptor distance. Yet, strikingly, we discovered the same trend in FRET when the bilayer thickness was increased at constant surface density of the protein. We also recombined equimolar Rho-Alexa 488 and Rho-Alexa 594 pairs with phosphatidylcholines (PCs) having unsaturated acyl lengths ranging from 14 to 24 carbons, with a nominal protein/lipid molar ratio of 1:100 (Fig. 1 *f*). It is known from ^{2}H NMR studies that the bilayer thickness increases with the phospholipid acyl chain length (36). All membranes were in the liquid-crystalline state, with the possible exception of di(24:1)PC ($T_m = 24$°C). A systematic reduction in the donor excitation intensity at 485 nm and greater emission at 515 nm occurred, accompanied by a loss of acceptor emission at 620 nm, similar to dilution of the labeled rhodopsin molecules within the membrane.

Influences of crowding of rhodopsin and hydrophobic mismatch

Next, we calculated the energy transfer efficiency (*E*) between the donor and acceptor rhodopsin fluorophores from the excitation and emission spectra. Values of *E* ranged from approximately zero, indicating essentially complete protein dispersal within the ca. 60-Å Förster radius of the Alexa fluorophores, to nearly 0.3, an appreciable value. A graph of *E* as a function of the protein/lipid molar ratio (Fig. 2 *a*) showed a dramatic increase as rhodopsin became more densely packed or crowded within the membrane. The increase in FRET was greater than the background calculated for a random distribution of donor and acceptors with appropriate values for the Förster radius R_0 and orientation factor κ^2 (37), and indicated nonideal mixing of the rhodopsin molecules.

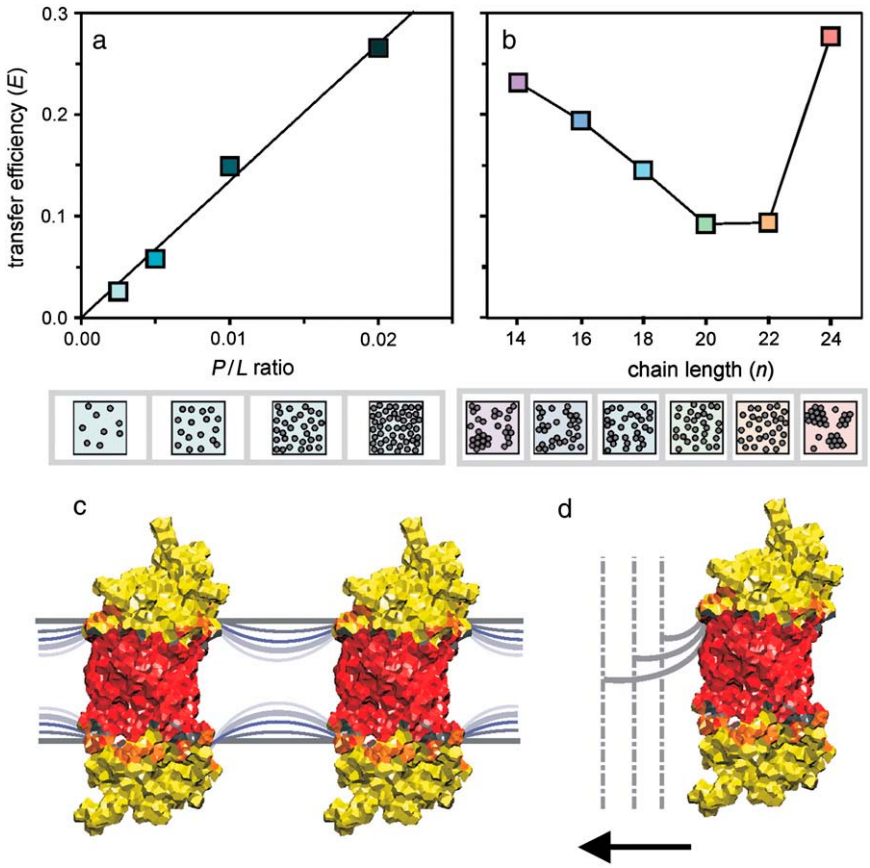

FIGURE 2 Curvature mismatch drives association of rhodopsin in fluid membranes. (*a* and *b*) FRET efficiency (*E*) plotted against (*a*) protein/lipid ratio and (*b*) increasing acyl chain length (*n*) for rhodopsin recombined with unsaturated PCs. Lines through data are to guide the eye and do not assume a specific functional form. (Data for $n = 24$ may include a contribution from gel-state lipids (cf. text).) Schematic depictions of the effects of bilayer thickness and protein/lipid ratio on receptor association are shown beneath the plots and correspond to the relative areas of proteins and lipids (14). (*c*) Illustration of how curvature affects membrane protein energetics by capillary forces. Curvature free energy is relieved by association of a fraction of the protein into clusters or microdomains (cf. text). (*d*) Illustration of how greater mismatch of lipid bilayer thickness to the protein hydrophobic length creates increased curvature of the proteolipid neutral boundary surface, which favors a larger optimum protein separation.

Moreover, for rhodopsin in the homologous di(*n*:1)PC series, a similar diminution of *E* was found with increasing acyl length (*n*) (Fig. 2 *b*). A bilayer thickness corresponding to $n \approx 20$–22 acyl carbons or greater was optimal for maintaining receptor dispersal within the membrane, e.g., due to solvating the hydrophobic protein surface. As the average donor and acceptor surface densities are essentially the same, the changes in *E* are explained by nonideal (nonrandom) mixing of receptors over distances of ca. 60 Å during the nanosecond fluorescence lifetime. The increase in *E* for rhodopsin in di(24:1)PC membranes may reflect that experiments were conducted below the gel-to-liquid-crystal transition temperature of $T_m = 24°C$, since control experiments at 28°C gave a reduction (not shown). In the gel state, the bilayer thickness is greater and the interfacial area/lipid is less than in the fluid or liquid-crystalline (L_α) state. Our interpretation is consistent with previous studies of rhodopsin-lipid interactions employing freeze-fracture electron microscopy (38) and saturation-transfer spin-label electron paramagnetic resonance (EPR) spectroscopy (24), which provide evidence for rhodopsin association as a function of protein/lipid ratio, acyl chain length, and lipid phase state. We note that an optimal chain length for protein dispersal, as measured by the rotational correlation time of rhodopsin, has been observed in previous EPR spin-label studies of recombinants with saturated PCs (see below) (24,25).

Our experimental design allowed us to deduce that *E* included significant effects from nonideal mixing of the rhodopsin molecules, due to clustering and/or microdomain formation. The fact that increasing the protein concentration and decreasing the lipid acyl length yield similar effects on FRET, with transfer efficiencies *E* that exceed the random background (37), argues that both are affected by the same mechanism. For ideal mixing, a simple biexponential dependence of *E* on the 2D surface density of acceptors is expected (37) (not shown). Expanding the predicted dependence in a Taylor series to linear order gives $E \propto P/L$, which agrees with the results in Fig. 2 *a*. However, including the data of Fig. 2 *b*, where the protein/lipid ratio is constant, makes it clear that a highly nonmonotonic dependence is in fact the case. As we could not explain the dependence of FRET on the fluorophore surface density by assuming ideal mixing, the distances between proteins were not calculated (37). We also note that our thermodynamic analysis does not include any specific molecular details of the protein packing in the bilayer. However, extension of the Förster theory to include nonideal mixing by formation of microdomains or clusters of receptor molecules allows some further general conclusions to be drawn. Briefly, we apply a simple two-state model that separates the acceptor surface density into contributions from receptors that are either dispersed or associated. The energy transfer efficiency of the dispersed fraction depends on the

acceptor surface density as described previously (37). On the other hand, E of the condensed protein complexes is assumed to be approximately constant. The resulting transfer efficiency curves include both contributions, with a break at the critical surface concentration, viz., protein/lipid ratio. The onset of clustering occurs at the critical surface density, above which there is an increase in E beyond the value for ideal mixing. Qualitatively, this simple model is successful in explaining (i), the large increase in E with increasing protein/lipid ratio (Fig. 2 *a*); and (ii), the corresponding increase in E with decreasing bilayer thickness (Fig. 2 *b*). At present, we do not attempt to estimate cluster sizes or distance distributions, which requires more extensive experimental data.

Studies of the effects of bilayer thickness on membrane proteins include investigations of rhodopsin (24,25,27,38,39), bacteriorhodopsin (40,41), Ca^{2+}ATPase (42), and mechanosensitive channels (43), reviewed in Lee (42) and Jensen and Mouritsen (44). An influence of bilayer thickness is consistent with models for hydrophobic matching in terms of membrane protein solvation (24,25,27,39). However, solvating the nonpolar residues of rhodopsin by the lipid chains involves the molecular surface area, and it is relatively short-range. Likewise, the hydrophobic effect involves cagelike structures about nonpolar groups, mainly by first-shell waters (45). An alternative view is that the lipid coherence (persistence) length can render the protein energetics sensitive to elastic deformation of the membrane film (27,31,44,46). One way to differentiate the two hypotheses entails changing the protein/lipid molar ratio. Fig. 2 *c* is an heuristic illustration of how elastic membrane deformation is coupled to the protein inclusion. Membranes at equilibrium in the absence of osmotic pressure have no lateral tension (stress). The monolayer spontaneous curvature H_0 represents a balance of forces involving the polar headgroups and the acyl chains (the lateral pressure profile). The value of H_0 can be directly measured for membrane lipids in the presence of hydrophobic solutes that reduce the chain packing energy holding the two monolayers together (27). It can be negative (curvature toward water, as in reverse H_{II} phase lipids), zero (as for planar PC bilayers), or positive (curvature toward hydrocarbon, as in the normal H_I phase), cf. Fig. 11 of Brown (27). Hydrophobic matching of the nonpolar protein surface to the bilayer imposes significant curvature H at the proteolipid boundary (27,31,47). Curvature and hydrophobic matching are not independent quantities, as shown by the curves in Fig. 2 *c*. Rather, a greater difference in hydrophobic length of the protein versus the bilayer gives a large curvature (strain). We propose that the competition of the curvature strain and hydrophobic matching favors an increased protein separation (Fig. 2 *d*), which yields condensation of a separate protein-rich phase involving clusters or microdomains, as further discussed below. Hence, the critical membrane property is the curvature mismatch $|H - H_0|$; the contact angle at the protein-lipid boundary is approximately the same, and solvation or wetting of the protein surface (hydrophobic matching) remains unaltered. Deformation of the bilayer provides a source of work that drives changes in protein or lipid clustering, or conformational changes linked to membrane protein functions.

Photoactivation of rhodopsin is governed by nonspecific membrane properties

An important aspect pertains to an area that has attracted much recent interest, that is, the role of membrane lipids in modulating signal transduction and other biological functions. Our aim was to observe how the FRET efficiency of donor-acceptor pairs of the fluorescent rhodopsin conjugates was correlated with effects of the membrane lipid composition on receptor function. UV-visible absorption changes were measured based on a pH-step method that involved high actinic light intensity (89 ± 7% bleaching) (cf. Supplementary Material). The initial pH of the sample was set to 6, which stabilized the active MII photoproduct of rhodopsin, and minimized isorhodopsin formed by secondary photolysis (48,49). After exposure to the actinic light, a rapid pH step to more alkaline values gave a shift of the equilibrium from active MII to the inactive MI state (Fig. 3 *a*). A combination of the ionophores CCCP and valinomycin was introduced for fast pH equilibration across the membrane. Calculation of the fraction (θ) of photoproducts with a deprotonated Schiff base (50,51) entailed difference spectrophotometry (Fig. 3 *b*). We first measured a full pH titration curve for rhodopsin/POPC (1:100) membranes from pH 4−10, which revealed three separate transitions (Fig. 3 *c*). The usual MI-to-MII equilibrium was observed near neutral pH (48), together with protonation of MII at acidic pH values (52) and deprotonation of MI at alkaline pH (18). The entire titration curve was fit numerically to Eq. 2 with three independent pK_a values (pK_{a1}, pK_{a2}, and pK_{a3}), according to the following chemical equilibrium:

$$\mathrm{MII_{PSB}} \underset{(1)}{\overset{-\mathrm{H}^+}{\rightleftharpoons}} \mathrm{MII_{SB}} \underset{(2)}{\overset{-\mathrm{H}^+}{\rightleftharpoons}} \mathrm{MI_{PSB}} \underset{(3)}{\overset{-\mathrm{H}^+}{\rightleftharpoons}} \mathrm{MI_{SB}}. \qquad (3)$$

Here, PSB indicates an N-retinylidene chromophore with a protonated Schiff base linkage ($\lambda_{max} \approx 480$ nm), whereas SB denotes the corresponding deprotonated Schiff base ($\lambda_{max} \approx$ 380 nm). Three protons are taken up sequentially with different pK_a values. Alternatively, the data were fit from pH 5.5–8.5 by disregarding pK_{a1} and considering only pK_{a2} and pK_{a3} (Fig. 3 *c*). For rhodopsin in the dark state, 11-*cis*-retinal is an inverse agonist and the pK_a of the retinylidene protonated Schiff base is >16. Upon photolysis, the pK_a for deprotonation of MI is reduced to 7.8 and for MII it is ca. 4 (52). In terms of these pK_a shifts, the chromophore evolves progressively to become a full agonist in the MII state, where the Schiff base nitrogen is deprotonated. We propose that this may represent the behavior of GPCRs in general, where typically a ligand does not activate the receptor immediately, but rather a partial activation occurs followed by rearrangement to the fully activated receptor.

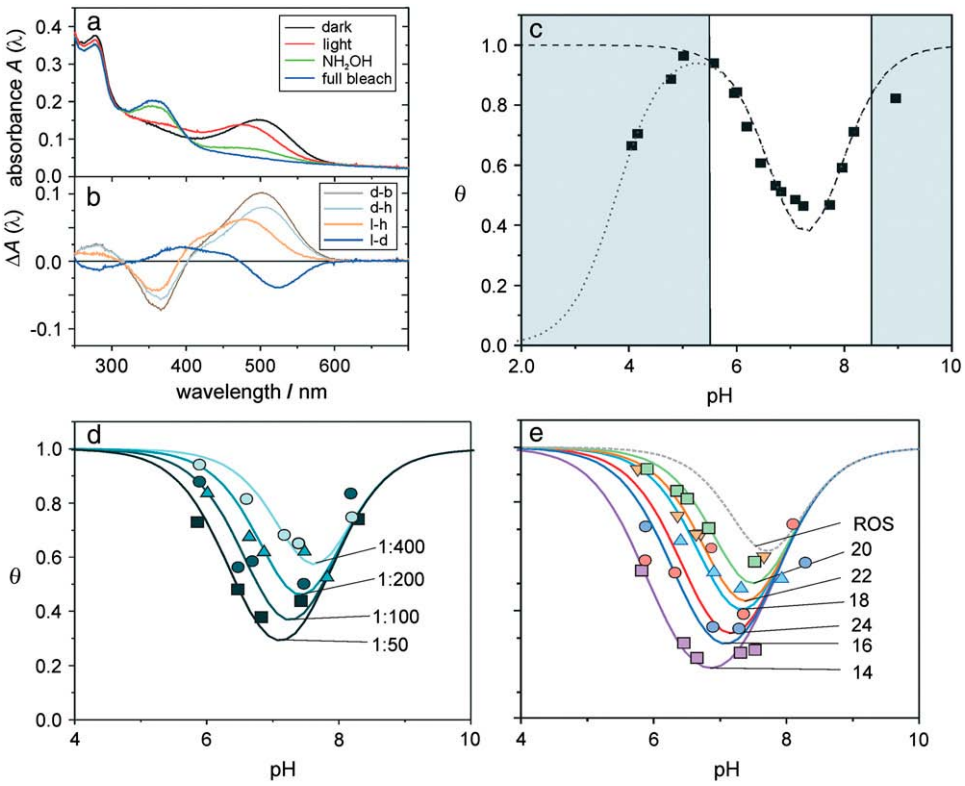

FIGURE 3 Activation of rhodopsin is governed by chemically nonspecific properties of the bilayer. (*a*) Representative UV-visible spectra of rhodopsin in di(14:1)PC membranes ($P/L = 1{:}100$) at pH 6.6 and 20°C. The spectral sequence is dark (*d*, *black*), light (*l*, *red*), addition of hydroxylamine (*h*, *green*), and fully bleached (*b*, *blue*) (descending order at 500 nm). (*b*) The corresponding difference spectra. (*c*) Fraction (θ) of Schiff base deprotonated photoproducts (MI and MII) for rhodopsin/POPC membranes ($P/L = 1{:}100$) at 20°C over pH range 4–10. Data are fit either with three separate pK_a values (*dotted line*) ($pK_{a1} = 3.8$, $pK_{a2} = 6.8$, $pK_{a3} = 7.8$); or two pK_a values (*dashed line*) omitting data for pH <5 ($pK_{a2} = 6.8$, $pK_{a3} = 7.8$). Solid lines delimit the pH range of typical measurements. (*d* and *e*) pH titration curves for (*d*) rhodopsin in POPC bilayers at 20°C as a function of protein/lipid ratio from 1:50 to 1:400 (colors as in Fig. 1 *e*) and (*e*) rhodopsin in di(*n*:1)PC membranes ($P/L = 1{:}100$) for different bilayer thickness (*n*) (colors as in Fig. 1 *f*). To increase robustness of the fits, only pK_{a2} is varied holding $pK_{a3} = 7.8$.

We then extended the approach to recombinant membranes differing in their rhodopsin/lipid ratio or acyl chain length (Fig. 3, *d* and *e*). In all cases, it was assumed that the reaction described by the equilibrium in Eq. 3 was applicable. Due to the range of systems investigated, the data are more sparse than for the rhodopsin/POPC (1:100) membranes (Fig. 3 *c*). The scatter most likely derives from random errors in the UV-visible spectral measurements (cf. Supplementary Material). However, by constraining the experimental data to fit Eq. 2, the analysis becomes more robust than otherwise. We studied influences of both the rhodopsin/lipid molar ratio (Fig. 3 *d*) and the bilayer thickness (Fig. 3 *e*) on the UV-visible spectral behavior over the pH 6–8 range. Our data extend experiments at single pH values, where different protiated forms of MI and MII were not distinguished (50,51). In all cases, the standard Levenberg-Marquardt gradient expansion algorithm was used for nonlinear regression fitting of the data, where the errors in the fitting parameters are proportional to the inverse curvature matrix of the χ^2 hypersurface. To further increase the robustness of the fitting, we reduced the number of free parameters (degrees of freedom) in the analysis. Only pK_{a2} was varied, whereas $pK_{a3} = 7.8$ was frozen, since it was approximately unaffected by the lipid composition. Fig. 3, *d* and *e*, shows that either a reduction in close packing of rhodopsin, due to a smaller protein/lipid molar ratio, or an increase in the bilayer thickness gave an increase in pK_{a2} that correlated with greater membrane dispersal in the FRET experiments. The FSM provides a mechanistic interpretation of the influences of membrane lipids on the energetics of photolyzed rhodopsin and its dispersal in the bilayer, as further described below.

Molecular mechanism of photoreceptor activation

First, we consider a molecular picture to account for the sequence of photolyzed rhodopsin states in Eq. 3, which are affected by properties of the membrane lipid bilayer. It is known that formation of the active MII state of rhodopsin involves two distinct protonation steps (3). The first involves the retinylidene Schiff base of helix H7 in close proximity to the counterion Glu^{113} located in helix H3, and involves breaking an ionic lock in conjunction with receptor activation. (Alternatively, a complex counterion involving the carboxylates of Glu^{113} and Glu^{181} can be considered (12,53).) The second protonation site has been proposed to be Glu^{134}, which is found in the conserved E(D)RY motif of family A GPCRs, and is contiguous to Arg^{135} in helix H3 (14,54). Breaking the salt bridges between the retinylidene Schiff base in helix H7 and residues in the H3/H6 domain leads to receptor activation. It follows that we consider the four species MII_{PSB}, MII_{SB}, MI_{PSB}, and MI_{SB}, which are conjugate acids or bases that differ from one another by the release or acceptance of a proton. Activation of the photoreceptor ''unlocks'' two salt bridges, one involving the H3/H6 helical domain and the other between helices H3 and H7.

Below, the left side of the symbol // indicates a salt bridge (. . .) between the Schiff base and Glu^{113}, and the right side refers to a salt bridge between the Glu^{134} and Arg^{135} residues:

MII_{PSB}^{+2}:

$$\text{retinal}-C=NH^{+}-Lys^{296}Glu^{113}H//Glu^{134}H\ Arg^{135+} \quad (4a)$$

MII_{SB}^{+}:

$$\text{retinal}-C=\ddot{N}-Lys^{296}Glu^{113}H//Glu^{134}H\ Arg^{135+} \quad (4b)$$

MI_{PSB}:

$$\text{retinal}-C=NH^{+}-Lys^{296}\ldots Glu^{113-}//Glu^{134-}\ldots Arg^{135+} \quad (4c)$$

MI_{SB}^{-1}:

$$\text{retinal}-C=\ddot{N}-Lys^{296}Glu^{113-}//Glu^{134-}\ldots Arg^{135+}. \quad (4d)$$

Beginning with MII_{PSB} at acidic pH values (Eq. 4a) the retinylidene Schiff base becomes deprotonated in MII_{SB} (Eq. 4b) due to transfer of a hydronium ion to the aqueous medium, whereas Glu^{113}, Glu^{134}, and Arg^{135} all remain protonated. At pH values around neutrality, protonation of the Schiff base occurs, whereas Glu^{113} is deprotonated giving an internal ion pair; in concert, Glu^{134} is deprotonated and forms a second ion pair with Arg^{135} in the MI_{PSB} state (Eq. 4c). Thus, the physiological transition from MI_{PSB} to MII_{SB} involves two partial reactions, in which two salt bridges are broken (Eqs. 4b and 4c). Last, at alkaline pH values, the retinylidene Schiff base is again deprotonated in the MI_{SB} state (Eq. 4d). For the overall reaction, the stoichiometry of protons is $n = 3$, as described by Eq. 3.

The reaction scheme that Eqs. 3 and 4 describe is a simple extension of the classical MI_{PSB}-to-MII_{SB} transition (48,55) to include different pK_a values for deprotonation of the retinylidene Schiff base in the MII and MI states. Breaking or ''unlocking'' the two internal salt bridges involving both helices H3 and H7 allows the conformation change from MI_{PSB} to MII_{SB} to be mechanically coupled to membrane deformation forces (31). An interesting finding is that certain lipids can shift the value of pK_{a2} for the transition from MI_{PSB} to MII_{SB} to ca. 7 or greater, as seen for rhodopsin in nonionic detergents with flexible chains (56). Another important feature is the presence of two spectrally silent photoproducts, MI_{SB} and MII_{SB}, which differ from previously described isochromic MII_{SB} forms (56). However, the thermodynamic model is not a detailed kinetic reaction mechanism in terms of elementary steps (17,56,57). Further studies of rhodopsin in membrane environments where the MI-to-MII equilibrium is perturbed can shed additional light on the reaction mechanism in the native system (17,56).

Flexible surface model for lipid-protein interactions

At this juncture, we recall that in its biological context, rhodopsin is a component of a supramolecular assembly, that is, comprising protein, phospholipids, and water. Above, we put forth a molecular explanation for the MI-to-MII transition at the level of the rhodopsin molecules. What are the corresponding properties of the membrane lipid bilayer that are implicated in activation of the photoreceptor? In fact, two approaches are possible in the mesoscopic regime between the molecular size and the bulk membrane dimensions. Either one can consider a molecular picture, or a continuum model can be introduced at various levels of detail. Let us next consider a continuum treatment of the bilayer in terms of its material properties (27), as an alternative to all-atom molecular dynamics simulations (14) or analytical molecular theories (58,59). Lack of reference to molecular detail is both a weakness and strength of the continuum elastic approach. Previous experimental work has shown the occurrence of clustering of rhodopsin and other membrane proteins (38, 40,50,51), as well as changes in rhodopsin function due to the lipid composition (27,31,39). Yet the physical origin and the types of intermolecular interactions remain an open question, particularly with regard to the length scale and the role of elastic stress and strain (frustration). Here, a combined approach employing both FRET and UV-visible spectrophotometry is adopted, since rhodopsin can be studied under nearly identical conditions over a wide range of pH, lipid composition, and protein/lipid molar ratio. Our results suggest that protein-lipid interactions extending beyond a single annulus of boundary lipids can play a crucial role in both rhodopsin clustering and function. Fig. 4 *a* shows that a continuous reduction in pK_{a2} was observed with increasing protein/lipid molar ratio, whereas pK_{a3} is approximately constant. An analogous increase in pK_{a2} was observed for unsaturated PCs as a function of acyl length up to ca. 20 or 22 carbons, beyond which pK_{a2} decreased with a slight reduction in pK_{a3} over the whole range (Fig. 4 *b*). (Results for 24-carbon chains may include contributions from gel-state lipids and are presented for completeness.) We note that the MI_{SB} state with a deprotonated Schiff base is typically observed only as a transient intermediate in time-resolved UV-visible spectrophotometry (60). According to Fig. 4 *b*, a relatively large difference in pK_{a2} and pK_{a3}, as in the case of 14-carbon chains, provides a means to study the MI_{SB} conformation near physiological temperature. Moreover, we discovered a relationship between the values of pK_{a2} for the MI-to-MII conformational change and the FRET efficiency for rhodopsin in the dark state (Fig. 4 *c*). These findings clearly establish that lipid-driven changes in protein packing density and excluded volume can govern the activity of a membrane protein.

Our studies provide a first meaningful experimental look at how rhodopsin function is influenced by its association state in fluid membranes. We propose that increasing protein concentration and decreasing bilayer thickness both affect rhodopsin by the same mechanism, which is due to a competition of curvature strain with hydrophobic matching. Frustration of the lipid bilayer curvature free energy due to

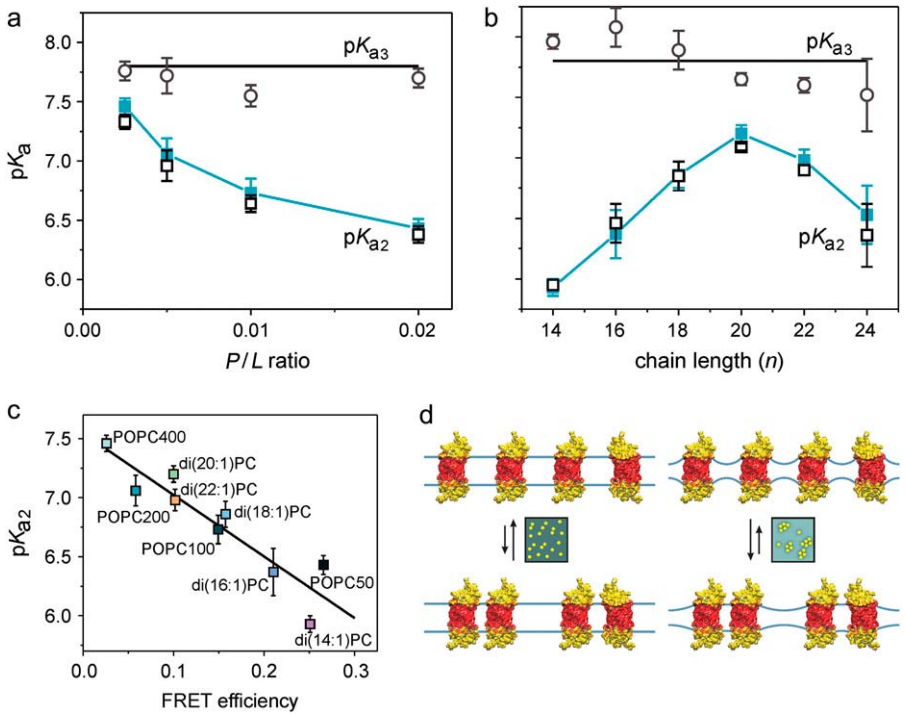

FIGURE 4 Photoactivation of rhodopsin is correlated with its packing density in fluid membranes. (*a*) Dependence of pK_{a2} and pK_{a3} values for MI-to-MII transition of rhodopsin/POPC membranes on protein/lipid molar ratio at 20°C. (*b*) Variation of pK_{a2} and pK_{a3} for MI-to-MII transition of rhodopsin in di(*n*:1)PC membranes ($P/L = 1{:}100$) on acyl length (*n*) at 20°C. (Data for $n = 24$ may include gel-state lipids (cf. text).) Solid lines and symbols are for one-parameter fits to pK_{a2} freezing p$K_{a3} = 7.8$; and open symbols are two-parameter fits allowing both pK_{a2} and pK_{a3} to vary. The experimental errors correspond to the fits in Fig. 3, *d* and *e*. (*c*) Values of pK_{a2} for MI-to-MII transition obtained from fitting UV-visible spectral data plotted against FRET efficiency at 20°C. (Data for di(24:1)PC membranes are excluded since experiments are below T_m.) (*d*) Illustration of how curvature matching of membrane bilayer to photoreceptor can drive association or dispersal linked to protein activity (capillary condensation). Equilibrium between dispersed (*top row*) and associated (*bottom row*) rhodopsin is depicted for PC bilayers ($H_0 \approx 0$) (cf. text). Wetting of the hydrophobic protein surface, together with membrane curvature, leads to protein association described by FSM.

interactions with rhodopsin has been discussed within the framework of a flexible surface model (27,31,55). We now extend these ideas based on the continuum theory of membrane elasticity (26) to account for changes in the lateral distribution of receptors associated with bilayer deformation forces. The FSM (31) offers a simple explanation in terms of elastic membrane deformation, and is connected with more extensive theoretical treatments (44,46,47,59,61–63), as reviewed in Jensen and Mouritsen (44). It builds on concepts from surface chemistry and physics (nanotechnology), in which emergent properties bear a direct correspondence to experimental observables. Due to the complexity of lipid packing in biomembranes (14), we use a simple continuum description in terms of phenomenological material constants. We introduce the spontaneous curvature H_0 and the monolayer bending rigidity k_c (related to the lateral compressibility k_a for pure planar strain) to relate our experimental measurements to theoretical concepts. Mismatch of the curvature H at the proteolipid boundary (Fig. 2 *d*) to the spontaneous monolayer curvature H_0 of the lipids frustrates the bending free energy, which scales as $k_c|H - H_0|^2$. The spontaneous monolayer curvature H_0 describes the balance of attractive and repulsive forces as a function of bilayer depth, and is related to the lateral pressure profile (64). It is formulated in terms of a neutral or dividing surface, where the curvature and area elastic deformation are decoupled or independent (27). For the present purposes, we focus on curvature deformation and assume that the neutral surface area is approximately constant (55). The Gaussian (saddle) curvature (27) is also neglected, to simplify the treatment.

The role of curvature in condensed matter with applications to membranes is reviewed elsewhere (65). Fig. 4 *d* illustrates how association of a fraction of the protein allows for greater expression of the spontaneous curvature in fluid membranes. At left, rhodopsin is depicted in a relatively thick bilayer ($H_0 \approx 0$); curvature H is small and dispersed receptors (*top*) are stabilized versus dimers or higher oligomers (*bottom*). At right, a relatively thin bilayer is shown with greater curvature (*top*), which drives protein association (*bottom*) to reduce elastic curvature deformation of the intervening lipid bilayer. Additional influences of membrane lipids may affect rhodopsin activation (22,31). According to the FSM, an optimal protein/lipid ratio for dispersal exists due to a balance of curvature and hydrophobic matching of the lipids to the protein (31), in analogy with wetting and capillary forces in surface and colloid chemistry (66). Analogous conclusions have been reached based on molecular theories (59). We suggest that the optimal protein/lipid ratio for dispersal is related to the critical protein surface density (see above), beyond which association of the receptor molecules occurs. Lipid-driven association of membrane proteins may thus be implicated in clustering or oligomerization of cellular membrane receptors.

DISCUSSION

Lipid-rhodopsin interactions have been discussed previously within the framework of a flexible surface model (27). Curvature elastic deformation due to long-range geometrical

forces, as originally put forth to explain lipid-protein interactions (31,55,67), has now attracted the attention of structural and cellular biologists (43,68–72). Investigations of membrane-bound enzymes (73,74), microorganism growth (75), and peptide ion channels (76) have all shown influences of chemically nonspecific bilayer properties on function. We now enlarge these principles to include changes in the lateral distribution and activation of receptors due to bilayer deformation forces. Chemically nonspecific properties of bilayer lipids affect the conformational energetics of rhodopsin, and explain their influences on its activation and related aspects of visual signal transduction. We discovered effects of the protein/lipid molar ratio on the lateral distribution of receptors that can help to clarify the role of membrane curvature forces and hydrophobic solvation in the case of rhodopsin. For hydrophobic matching (42,44,58, 77,78), the lipid influences on the protein are relatively short-range, and mainly involve the lipid/protein interface as in previous EPR spin-label studies (25,79). Yet changing the rhodopsin/lipid ratio affects both protein dispersal and its activation, so that interactions extending well beyond the annular or boundary lipids govern the membrane energetics. A possible explanation is that both the membrane bilayer and the protein inclusions have an inherent flexibility, thus allowing a mutual coupling of their free energies (27). Crowding of the receptors due to an increase in protein packing density yields a reduction in the activated MII state of rhodopsin, the signaling form. Why would greater association of rhodopsin in the membrane favor the occurrence of inactive photoproducts? It is known that the MI-to-MII transition involves an increase in partial molar volume, consistent with the helix-movement model of GPCR activation (4,80) and a restructuring of the membrane lipids (31), which could be inhibited by rhodopsin association. Assuming that active MII is a more expanded conformation than inactive MI, there could be an influence of excluded membrane volume due to steric repulsions among the proteins (crowding). This is similar to the observation that formation of the activated MII state is inhibited or blocked in densely packed 2D rhodopsin arrays (18,81,82) or 3D crystals (13). However, it differs from the recent proposal that activation of rhodopsin is enhanced by its association in micelles or membranes (83).

Rhodopsin association has been previously studied in recombinant membranes by employing freeze-fracture electron microscopy (38) and spin-label EPR spectroscopy (24,25). From these experimental studies, it can be concluded that association of rhodopsin occurs in recombinant membranes with PCs having different acyl chain lengths (24,25). Work with ^{2}H NMR spectroscopy has established that the bilayer thickness increases with the acyl chain length, as opposed to the cross-sectional area per lipid (36). Evidence for transient rhodopsin association in both recombinant and native membranes that depends on the lipid composition and protein content has been obtained using saturation-transfer spin-label EPR (24,25). Protein clustering or association is inferred from an increase in rotational correlation time, instead of an experimental quantity that is sensitive to the protein-protein distances. Using EPR, an optimal bilayer thickness has been found for dispersal of rhodopsin in the case of saturated PC recombinants, which corresponds to an acyl chain length of ca. 15–16 carbons. However, for saturated PCs, comparison needs to be done at different temperatures due to the high melting points of the saturated acyl chains. By contrast, the present FRET experiments employ recombinants of rhodopsin with unsaturated PCs, and they detect protein association directly over a larger range of protein/lipid molar ratios. In this case, we find a somewhat greater optimal bilayer thickness, corresponding to a ca. 20- or 22-carbon acyl length or longer. The apparent discrepancy of the chain-length optimum found in our experiments with the earlier EPR spin-label data may be due to a larger bilayer thickness in the case of saturated PCs versus unsaturated PCs for equivalent acyl chain lengths (84). An important technical aspect is that our work has employed rhodopsin/lipid membranes prepared by dialysis from a mixture of octylglucoside and cholate detergents. Recombinant membranes formed by dialysis from octylglucoside alone are inhomogeneous with respect to the protein/lipid ratio, thus potentially invalidating the results. However, in agreement with previous accounts (24,25,33), we find that inclusion of cholate leads to good control of the protein/lipid ratio, as assessed by isopycnic density gradient centrifugation together with enzymatic phospholipid determination (cf. Supplementary Material).

New biomembrane model: curvature elastic deformation

The FSM is reviewed elsewhere (27), and here we provide a brief recapitulation for those readers who may not be familiar with the earlier development. To paraphrase Gibbs, we wish to find the point of view from which the subject of lipid-protein interactions appears in its greatest simplicity. The central idea involves extending the concept of the monolayer curvature free energy (26) to the mesoscopic length scale that is characteristic of lipid-protein interactions. By contrast, the standard fluid-mosaic model found in textbooks states that the lipid bilayer acts as a permeability barrier, and is mainly a structural element or matrix for the organization of membrane proteins. According to the standard model the lipids do not play any direct role in the activities of proteins. The alternative is that membrane lipids are implicated in the protein-mediated functions of biomembranes (27,42,44), a view that is supported by the data presented here.

In the case of membrane lipids and surfactants, there is a balance of opposing forces involving the polar headgroups and the hydrocarbon tails that is connected with their nanostructures and polymorphism (65,85). Headgroup repulsions and interfacial attraction give an optimal separation

for the polar region, and within the hydrocarbon core, van der Waals attraction plus steric repulsion give a preferred distance between the chains (85). Rather than explicitly considering the detailed form of the lateral pressure profile, we simply introduce the resultant bending moment in terms of a neutral surface where the curvature and area elastic deformation are decoupled. Relatively small lipid headgroups with a propensity for hydrogen bonding favor a condensation of the bilayer surface, whereas bulky or large acyl chains give a larger chain cross-sectional area, and vice versa. When the optimal separations for the polar headgroups and nonpolar chains differ, a bending moment or spontaneous curvature is the result. The balance of opposing forces within the polar headgroup region and the hydrocarbon region gives rise to the nanostructures and polymorphism of membrane lipids, encompassing the inverse hexagonal (H_{II}), fluid lamellar (L_α), cubic, and normal hexagonal (H_I) phases (65,66,85).

Obviously, for planar bilayers the geometrical curvature $H = 0$, so how is bending relevant in the present context? Here, one must appreciate that an elastic curvature strain can exist even in the case of a planar membrane, viz., in the absence of significant bilayer curvature. We emphasize that the resultant spontaneous curvature H_0 or bending moment of the lipid film does not necessarily correspond to the actual geometrical curvature H. Bending the surface away from the spontaneous curvature, which can be negative (toward water), positive (toward hydrocarbon), or zero, gives rise to a curvature elastic energy. In fact, a significant curvature elastic deformation can exist that is given by $k_c|H - H_0|^2$, where k_c is the bending rigidity or curvature elastic modulus, in direct analogy with Hooke's law for stretching a 1D spring from its equilibrium length. One must always keep in mind the distinction between the spontaneous curvature H_0 and the actual geometrical curvature H. In the FSM, both curvature matching at the proteolipid boundary and hydrophobic matching play a role in the energetics of membrane protein inclusions, and are connected with their biological functions.

Free energy coupling mechanism for rhodopsin

In the FSM, we focus mainly on the competition between long-range curvature elastic forces and the solvation energy of the protein/lipid interface. The solvation energy is due to hydrophobic mismatch of the acyl chains to the protein surface and is relatively short-range; it mainly involves the accessible surface area of the molecules. We have proposed that competition of the long-range curvature force with hydrophobic matching accounts for the influences of membrane lipids on protein conformational energetics and organization in biomembranes (27). Changes in hydrophobic matching are in turn coupled to changes in the curvature free energy. It is the balance of the two terms that explains how membrane lipids can govern the energetics of membrane proteins such as rhodopsin (31). We note that the energies of the bilayer deformation can be rather appreciable, far exceeding those implicated in typical protein conformational changes. Considering rhodopsin as a canonical membrane protein, we can postulate that the conformational changes implicated in the triggering of visual function entail an increase in the intramembranous hydrophobic surface (hydrophobic mismatch). A protrusion of the receptor from the membrane occurs due to exposure of recognition sites for the G-protein (transducin) (86). The MI-to-MII transition is favored by increasing acyl chain length, and also by the presence of lipids with a tendency to form the nonlamellar H_{II} phase (31). However, the new and unanticipated finding in this work is that the transition is also sensitive to the protein/lipid ratio (28).

Here, we propose that the various lipid influences all share a common origin, which resides in chemically nonspecific properties as described by the FSM. Due to the boundary condition of hydrophobic matching at the protein/lipid interface, a change in hydrophobic solvation is accompanied by a change in curvature strain (27). As a result, there can be a subtle but energetically significant competition between the elastic curvature energy of the membrane lipid film and the hydrophobic matching of the acyl chains to the protein hydrophobic surface. The two free energy terms cannot be simultaneously minimized, a concept that we refer to as frustration (55). This renders the membrane protein sensitive to chemically nonspecific properties of the bilayer, such as the spontaneous curvature of the membrane lipids. It follows that the lowest energy state of the membrane is one in which the curvature free energy of the lipid film is balanced by the solvation energy of the lipid/protein interface. For rhodopsin, the free energy balance of the receptor and the lipids is altered by photoisomerization of the retinylidene chromophore. Bleaching leads to the MI-to-MII transition, which involves an alteration of the free energy balance due to the curvature elastic stress/strain and the degree of hydrophobic mismatch of the membrane (frustration). A new biophysical principle is introduced: matching of the spontaneous curvature of the lipid bilayer to the mean curvature of the lipid/water interface adjacent to the protein. Biological activity is thus regulated by membrane lipids whose spontaneous curvature most closely matches the active state of the proteolipid assembly.

Nonideal mixing and crowding of membrane proteins

In the case of fluid membranes, characteristic properties are linked with their lipid compositions and can affect the activities of membrane proteins, as discussed above for rhodopsin (27). Studies of mechanosensitive ion channels (43) have revealed analogous lipid influences, thereby further suggesting the generality of the principles first derived by investigating rhodopsin (27,55). The FSM is based on studies of surfactants and phospholipids, where curvature deformation

and elasticity are key to understanding their phase equilibria and nanostructures (87–89). For retinal rod membranes and other neuronal membranes, tightly regulated polyunsaturated lipids of the ω-3 class are known to play a crucial role (22,27,67). The conformational energetics of photolyzed rhodopsin are highly dependent on the membrane lipid or detergent environment (31,39,55,90), and influences of the rhodopsin/lipid ratio have been recently substantiated by us (28,29) and others (91). In our work, a positive correlation was found between a lipid environment where rhodopsin is relatively well dispersed and the activated MII conformation formed upon illumination. Nonideal mixing due to the membrane lipid composition leads to crowding of receptors, which can control membrane protein activity through steric repulsions and excluded volume in fluid membranes. It is worth noting that our thermodynamic picture does not include any specific structural representation of the system (27,31,55). However, plasmon (waveguide) resonance (PWR) spectroscopy gives direct evidence for an elongation of rhodopsin in connection with the MI-to-MII transition, together with a pre-coupling to transducin (G_t) and a dynamical restructuring of the lipid bilayer (86). Interaction of rhodopsin with bilayer lipids leads to alteration of the binding of transducin as demonstrated with PWR spectroscopy, which is linked to its signaling role as a GPCR in the visual system (92,93).

Curvature and hydrophobic forces in rhodopsin association

How does coupling of the lipid bilayer forces to rhodopsin drive conformational changes and receptor association in the membrane? The energetics of rhodopsin have been probed in relation to its photochemistry and activation (55,94,95) and with regard to interactions that stabilize the native protein structure (96,97). Lipid-mediated protein interactions in membranes have been considered theoretically (40,47,77) and experimental studies have been carried out for bacteriorhodopsin (40) and rhodopsin (24,38). We now further consider how long-range lipid-protein interactions due to curvature yield greater receptor crowding. It is known that capillary forces due to a curved interface lead to adherence of small particles as in the familiar case of wet sand grains, which is termed capillary condensation (66). For a conventional gas-liquid equilibrium with a curved interface, the hydrostatic pressure is greater on the concave side of the meniscus as described by the Young-Laplace equation, which is the basis for capillary action. This gives rise to capillary condensation in microporous materials and explains the formation of sandcastles. Equivalently, the chemical potential of a gas on the concave side is increased, corresponding to a lowering of the vapor pressure of the liquid as given by the Kelvin equation. Now in direct analogy, we can consider a membrane containing proteins dissolved in a bilayer that is treated as a continuous fluid. We assume that the protein has an equilibrium between a condensed or associated phase and a dispersed phase. The curvature free energy yields an increase in chemical potential of the proteolipid membrane (31), and as a result, the equilibrium can shift toward the condensed protein phase. We propose that curvature forces as described by a flexible surface model can lead to association of membrane proteins in fluid bilayers, e.g., into dimers and higher oligomers.

The FSM provides a simple framework based on surface chemistry for understanding how elastic deformation of the lipid bilayer can lead to a microenvironment of the membrane conducive for the receptor to function optimally (cf. Fig. 12 of Brown (27)). The new view entails consideration of lipid-protein interactions due to chemically nonspecific properties of the membrane in terms of a stress field extending beyond a single layer of annular or boundary lipids (27,31,46,55,98). Dispersal and activation of rhodopsin are explained by a balance of the monolayer curvature free energy together with hydrophobic coupling due to solvation or wetting of the protein intramembranous surface (27,55). In the FSM, the correlation length for lipid deformation appears naturally as the monolayer curvature, which is based on concepts of differential geometry (65). The spontaneous curvature H_0 is the resultant of a balance of geometrical forces (27) that is related to the lateral pressure profile along the normal direction to the bilayer interface, viz., as a function of bilayer depth (64,98). A key aspect of the FSM is that the influences of curvature and hydrophobic mismatch extend beyond the lipid/protein interface, due to elastic deformation of the membrane lipid film, thus exerting a mechanical force on the protein (31). The spontaneous curvature of a lipid monolayer acts together with hydrophobic mismatch to store elastic deformation energy within the bilayer, which can drive protein conformational changes, and possibly the formation of rhodopsin oligomers or microdomains. In this way, chemically nonspecific bilayer properties can lead to transduction of bilayer curvature and thickness deformation forces into membrane protein activity, thus providing a means of free energy coupling in biomembranes (31).

Oligomers of photoreceptors?

Much interest and commotion has focused recently on protein-protein interactions within the context of receptor oligomerization (2,5,6). Therefore, it is useful to ask the question, is association of rhodopsin as observed with FRET connected with formation of oligomers in native rod disk membranes? For rhodopsin, oligomerization has been brought to an issue by recent reports of atomic force microscopy (AFM) studies showing rows of dimers in native rod disk membranes (7,99). If substantiated by additional research, the implications for phototransduction and visual signaling would be quite profound (8,100). However, the proposed new paradigm of dimerization or oligomerization of rhodopsin and other GPCRs has been questioned (2,101) and

countered in detail (102). Yet another current view is that a monomer is the functional unit of rhodopsin and other GPCRs, both in membrane bilayers and in nonionic detergent micelles (2). At present, it appears that oligomerization of rhodopsin would contradict earlier equatorial x-ray diffraction data for native rod disk membranes, as well as neutron diffraction, hydrodynamic, and biochemical studies of rhodopsin in detergents (2). Even in the crowded disk membrane environment, the polyunsaturated membrane lipids support rapid rotational and translational diffusion of rhodopsin (24,101). Further, the organization of rhodopsin in membranes has been studied with freeze-fracture electron microscopy (38) and spin-label EPR (24), which do not support extensive oligomerization of the protein in the fluid lipid phase. By contrast, AFM yields clear evidence of rhodopsin association in native rod disk membranes (83,99,102,103). Additional investigations are needed in which the new FRET approach can play an important role.

Our work provides direct experimental evidence that the membrane lipid composition drives constitutive association or oligomerization of cellular receptors such as rhodopsin. Through understanding how membrane protein stability is elastically coupled to lipid bilayer forces, current paradigms for relating structure to function are brought into sharper focus. Receptor activation entails chemically nonspecific properties of the membrane lipid bilayer, which for rhodopsin are connected with its photochemical activity. Bilayer curvature deformation affects the protein energetics and stabilizes the active state conformation of the photoreceptor. Exactly how membrane protein stability is elastically coupled to lipid bilayer forces and how lipid rafts might be implicated in this process are the subjects of ongoing research.

SUPPLEMENTARY MATERIAL

An online supplement to this article can be found by visiting BJ Online at http://www.biophysj.org.

Note added in proof: While this article was in the review process, two related articles appeared (Kota, P., et al. 2006. *Proc. Natl. Acad. Sci. USA.* 103:3054–3059; Mansoor, S. E., et al. 2006. *Proc. Natl. Acad. Sci. USA.* 103:3060–3065).

We thank O. S. Andersen, M. Chabre, K. A. Dill, W. L. Hubbell, H. M. McConnell, and X. Periole for discussions.

This work was supported by the Ellison Medical Foundation and the Allene Reuss Memorial Trust (T.P.S.), and by the United States National Institutes of Health and National Aeronautics and Space Administration (M.F.B.). A.V.B. was awarded a research scholarship from CAPES, Brazil.

REFERENCES

1. Pierce, K. L., R. T. Premont, and R. J. Lefkowitz. 2002. Seven-transmembrane receptors. *Nat. Rev. Mol. Cell Biol.* 3:639–650.
2. Chabre, M., and M. le Maire. 2005. Monomeric G-protein-coupled receptor as a functional unit. *Biochemistry.* 44:9395–9403.
3. Sakmar, T. P., S. T. Menon, E. P. Marin, and E. S. Awad. 2002. Rhodopsin: insights from recent structural studies. *Annu. Rev. Biophys. Biomol. Struct.* 31:443–484.
4. Hubbell, W. L., C. Altenbach, C. M. Hubbell, and H. G. Khorana. 2003. Rhodopsin structure, dynamics, and activation: a perspective from crystallography, site-directed spin labeling, sulfhydryl reactivity, and disulfide cross-linking. *Adv. Prot. Chem.* 63:243–290.
5. George, S. R., B. F. O'Dowd, and S. R. Lee. 2002. G-protein-coupled receptor oligomerization and its potential for drug discovery. *Nat. Rev. Drug Disc.* 1:808–820.
6. Bouvier, M. 2001. Oligomerization of G-protein-coupled transmitter receptors. *Nat. Rev. Neurosci.* 2:274–286.
7. Fotiadis, D., Y. Liang, S. Filipek, D. A. Saperstein, A. Engel, and K. Palczewski. 2003. Rhodopsin dimers in native disc membranes. *Nature* (*Lond.*). 421:127–128.
8. Park, P. S.-H., S. Filipek, J. W. Wells, and K. Palczewski. 2004. Oligomerization of G protein-coupled receptors: past, present, and future. *Biochemistry.* 43:15643–15656.
9. Hernanz-Falcón, P., J. M. Rodriguez-Frade, A. Serrano, D. Juan, A. del Sol, S. F. Soriano, F. Roncal, L. Gómez, A. Valencia, C. Martínez-A, and M. Mellado. 2004. Identification of amino acid residues crucial for chemokine receptor dimerization. *Nat. Immunol.* 5:216–223.
10. Edidin, M. 2003. The state of lipid rafts: from model membranes to cells. *Annu. Rev. Biophys. Biomol. Struct.* 32:257–283.
11. Simons, K., and W. L. C. Vaz. 2004. Model systems, lipid rafts, and cell membranes. *Annu. Rev. Biophys. Biomol. Struct.* 33:269–295.
12. Yan, E. C. Y., M. A. Kazmi, Z. Ganim, J.-M. Hou, D. Pan, B. S. W. Chang, T. P. Sakmar, and R. A. Mathies. 2003. Retinal counterion switch in the photoactivation of the G protein-coupled receptor rhodopsin. *Proc. Natl. Acad. Sci. USA.* 100:9262–9267.
13. Okada, T., Y. Fujiyoshi, M. Silow, J. Navarro, E. M. Landau, and Y. Shichida. 2002. Functional role of internal water molecules in rhodopsin revealed by x-ray crystallography. *Proc. Natl. Acad. Sci. USA.* 99:5982–5987.
14. Huber, T., A. V. Botelho, K. Beyer, and M. F. Brown. 2004. Membrane model for the GPCR prototype rhodopsin: hydrophobic interface and dynamical structure. *Biophys. J.* 86:2078–2100.
15. Li, J., P. C. Edwards, M. Burghammer, C. Villa, and G. F. X. Schertler. 2004. Structure of bovine rhodopsin in a trigonal crystal form. *J. Mol. Biol.* 343:1409–1438.
16. Salgado, G. F. J., A. V. Struts, K. Tanaka, N. Fujioka, K. Nakanishi, and M. F. Brown. 2004. Deuterium NMR structure of retinal in the ground state of rhodopsin. *Biochemistry.* 43:12819–12828.
17. Szundi, I., T. L. Mah, J. W. Lewis, S. Jäger, O. P. Ernst, K. P. Hofmann, and D. S. Kliger. 1998. Proton transfer reactions linked to rhodopsin activation. *Biochemistry.* 37:14237–14244.
18. Ruprecht, J. J., T. Mielke, R. Vogel, C. Villa, and G. F. X. Schertler. 2004. Electron crystallography reveals the structure of metarhodopsin I. *EMBO J.* 23:3609–3620.
19. Salgado, G. F. J., A. V. Struts, K. Tanaka, S. Krane, K. Nakanishi, and M. F. Brown. 2006. Solid-state ^{2}H NMR structure of retinal in metarhodopsin I. *J. Am. Chem. Soc.* 128:11067–11071.
20. Borhan, B., M. L. Souto, H. Imai, Y. Shichida, and K. Nakanishi. 2000. Movement of retinal along the visual transduction path. *Science.* 288:2209–2212.
21. Patel, A. B., E. Crocker, M. Eilers, A. Hirshfeld, M. Sheves, and S. O. Smith. 2004. Coupling of retinal isomerization to the activation of rhodopsin. *Proc. Natl. Acad. Sci. USA.* 101:10048–10053.
22. Niu, S.-L., D. C. Mitchell, S.-Y. Lim, Z.-M. Wen, H.-Y. Kim, N. Salem, Jr., and B. J. Litman. 2004. Reduced G protein-coupled signaling efficiency in retinal rod outer segments in response to *n*-3 fatty acid deficiency. *J. Biol. Chem.* 279:31098–31104.
23. Kenworthy, A. K., N. Petranova, and M. Edidin. 2000. High-resolution FRET microscopy of cholera toxin B-subunit and GPI-anchored proteins in cell plasma membranes. *Mol. Biol. Cell.* 11:1645–1655.
24. Kusumi, A., and J. S. Hyde. 1982. Spin-label saturation-transfer electron spin resonance detection of transient association of rhodopsin in reconstituted membranes. *Biochemistry.* 21:5978–5983.

25. Ryba, N. J. P., and D. Marsh. 1992. Protein rotational diffusion and lipid/protein interactions in recombinants of bovine rhodopsin with saturated diacylphosphatidylcholines of different chain lengths studied by conventional and saturation-transfer electron spin resonance. *Biochemistry.* 31:7511–7518.
26. Helfrich, W. 1973. Elastic properties of lipid bilayers. Theory and possible experiments. *Z. Naturforsch.* 28c:693–703.
27. Brown, M. F. 1994. Modulation of rhodopsin function by properties of the membrane bilayer. *Chem. Phys. Lipids.* 73:159–180.
28. Botelho, A. V., T. Huber, and M. F. Brown. 2003. Flexible surface model for lipid-rhodopsin interactions: further analysis. *Biophys. J.* 84:55A (Abstr.).
29. Botelho, A. V., T. Huber, T. P. Sakmar, and M. F. Brown. 2005. Direct effect of membrane stress on lipid-rhodopsin organzation and function. *Biophys. J.* 88:579A (Abstr.).
30. Huber, T., A. V. Botelho, T. P. Sakmar, and M. F. Brown. 2006. Curvature and hydrophobic mismatch drive non-ideal mixing and activation of rhodopsin in membranes. *Biophys. J.* 90:15A (Abstr.).
31. Botelho, A. V., N. J. Gibson, Y. Wang, R. L. Thurmond, and M. F. Brown. 2002. Conformational energetics of rhodopsin modulated by nonlamellar forming lipids. *Biochemistry.* 41:6354–6368.
32. Borochov-Neori, H., and M. Montal. 1983. Rhodopsin in reconstituted phospholipid vesicles. 1. Structural parameters and light-induced conformational changes detected by resonance energy transfer and fluorescence quenching. *Biochemistry.* 22:197–205.
33. Borochov-Neori, H., P. A. G. Fortes, and M. Montal. 1983. Rhodopsin in reconstituted phospholipid vesicles. 2. Rhodopsin-rhodopsin interactions detected by resonance energy transfer. *Biochemistry.* 22:206–213.
34. Rajan, R. S., and R. R. Kopito. 2005. Suppression of wild-type rhodopsin maturation by mutants linked to autosomal dominant retinitis pigmentosa. *J. Biol. Chem.* 280:1284–1291.
35. Borochov-Neori, H., and M. Montal. 1989. Rhodopsin-G-protein interactions monitored by resonance energy transfer. *Biochemistry.* 28:1711–1718.
36. Petrache, H. I., S. W. Dodd, and M. F. Brown. 2000. Area per lipid and acyl length distributions in fluid phosphatidylcholines determined by ^{2}H NMR spectrscopy. *Biophys. J.* 79:3172–3192.
37. Wolber, P. K., and B. S. Hudson. 1979. An analytic solution to the Förster energy transfer problem in two dimensions. *Biophys. J.* 28: 197–210.
38. Hubbell, W. L. 1975. Characterization of rhodopsin in synthetic systems. *Acc. Chem. Res.* 8:85–91.
39. Baldwin, P. A., and W. L. Hubbell. 1985. Effects of lipid environment on the light-induced conformational changes of rhodopsin. 2. Roles of lipid chain length, unsaturation, and phase state. *Biochemistry.* 24:2633–2639.
40. Pearson, L. T., S. I. Chan, B. A. Lewis, and D. M. Engelman. 1983. Pair distribution-functions of bacteriorhodopsin and rhodopsin in model bilayers. *Biophys. J.* 43:167–174.
41. Lewis, B. A., and D. M. Engelman. 1983. Bacteriorhodopsin remains dispersed in fluid phospholipid bilayers over a wide range of bilayer thickness. *J. Mol. Biol.* 166:203–210.
42. Lee, A. G. 2004. How lipids affect the activities of integral membrane proteins. *Biochim. Biophys. Acta.* 1666:62–87.
43. Perozo, E., A. Kloda, D. M. Cortes, and B. Martinac. 2002. Physical principles underlying the transduction of bilayer deformation forces during mechanosensitive channel gating. *Nat. Struct. Biol.* 9:696–703.
44. Jensen, M. Ø., and O. G. Mouritsen. 2004. Lipids do influence protein function–the hydrophobic matching hypothesis revisited. *Biochim. Biophys. Acta.* 1666:205–226.
45. Dill, K. A., T. M. Truskett, V. Vlachy, and B. Hribar-Lee. 2005. Modeling water, the hydrophobic effect, and ion solvation. *Annu. Rev. Biophys. Biomol. Struct.* 34:173–199.
46. Nielsen, C., and O. S. Andersen. 2000. Inclusion-induced bilayer deformations: effects of monolayer equilibrium curvature. *Biophys. J.* 79:2583–2604.
47. Harroun, T. A., W. T. Heller, T. M. Weiss, L. Yang, and H. W. Huang. 1999. Theoretical analysis of hydrophobic matching and membrane-mediated interactions in lipid bilayers containing gramicidin. *Biophys. J.* 76:3176–3185.
48. Parkes, J. H., and P. A. Liebman. 1984. Temperature and pH dependence of the metarhodopsin I-metarhodopsin II kinetics and equilibria in bovine rod disk membrane suspensions. *Biochemistry.* 23:5054–5061.
49. Heck, M., S. A. Schädel, D. Maretzki, F. J. Bartl, E. Ritter, K. Palczewski, and K. P. Hofmann. 2003. Signaling states of rhodopsin. Formation of the storage form, metarhodopsin III, from active metarhodopsin II. *J. Biol. Chem.* 278:3162–3169.
50. van Breugel, P. J. G. M., P. H. M. Geurts, F. J. M. Daemen, and S. L. Bonting. 1978. Biochemical aspects of the visual process. XXXVIII. Effects of lateral aggregation on rhodopsin in phospholipase C-treated photoreceptor membranes. *Biochim. Biophys. Acta.* 509:136–147.
51. DeGrip, W. J., J. Olive, and P. H. M. Bovee-Geurts. 1983. Reversible modulation of rhodopsin photolysis in pure phosphatidylserine membranes. *Biochim. Biophys. Acta.* 734:168–179.
52. Vogel, R., G. B. Fan, F. Siebert, and M. Sheves. 2001. Anions stabilize a metarhodopsin II-like photoproduct with a protonated Schiff base. *Biochemistry.* 40:13342–13352.
53. Lüdeke, S., R. Beck, E. C. Y. Yan, T. P. Sakmar, F. Siebert, and R. Vogel. 2005. The role of Glu181 in the photoactivation of rhodopsin. *J. Mol. Biol.* 353:345–356.
54. Fahmy, K., T. P. Sakmar, and F. Siebert. 2000. Transducin-dependent protonation of glutamic acid 134 in rhodopsin. *Biochemistry.* 39: 10607–10612.
55. Gibson, N. J., and M. F. Brown. 1993. Lipid headgroup and acyl chain composition modulate the MI-MII equilibrium of rhodopsin in recombinant membranes. *Biochemistry.* 32:2438–2454.
56. Arnis, S., and K. P. Hofmann. 1993. Two different forms of metarhodopsin II: Schiff base deprotonation precedes proton uptake and signaling state. *Proc. Natl. Acad. Sci. USA.* 90:7849–7853.
57. Straume, M., D. C. Mitchell, J. L. Miller, and B. J. Litman. 1990. Interconversion of metarhodopsins I and II: a branched photointermediate decay model. *Biochemistry.* 29:9135–9142.
58. Mouritsen, O. G., and M. Bloom. 1984. Mattress model of lipid-protein interactions in membranes. *Biophys. J.* 46:141–153.
59. May, S., and A. Ben-Shaul. 1999. Molecular theory of lipid-protein interaction and the L_α-H_{II} transition. *Biophys. J.* 76:751–767.
60. Thorgeirsson, T. E., J. W. Lewis, S. E. Wallace-Williams, and D. S. Kliger. 1993. Effects of temperature on rhodopsin photointermediates from lumirhodopsin to metarhodopsin-II. *Biochemistry.* 32:13861–13872.
61. Dan, N., P. Pincus, and S. A. Safran. 1993. Membrane-induced interactions between inclusions. *Langmuir.* 9:2768–2771.
62. Kralchevsky, P. A., V. N. Paunov, N. D. Denkov, and K. Nagayama. 1995. Stresses in lipid membranes and interactions between inclusions. *J. Chem. Soc. Faraday Trans.* 91:3415–3432.
63. Aranda-Espinoza, H., A. Berman, P. Dan, P. Pincus, and S. Safran. 1996. Interaction between inclusions embedded in membranes. *Biophys. J.* 71:648–656.
64. Cantor, R. S. 1999. The influence of membrane lateral pressures on simple geometric models of protein conformational equilibria. *Chem. Phys. Lipids.* 101:45–56.
65. Hyde, S. T., S. Andersson, K. Larsson, Z. Blum, T. Landh, S. Lidin, and B. W. Ninham. 1997. The Language of Shape. The Role of Curvature in Condensed Matter: Physics, Chemistry and Biology. Elsevier, Amsterdam.
66. Evans, D. F., and H. Wennerström. 1999. The Colloidal Domain: Where Physics, Chemistry, Biology, and Technology Meet, 2nd Ed. Wiley-VCH, New York.
67. Wiedmann, T. S., R. D. Pates, J. M. Beach, A. Salmon, and M. F. Brown. 1988. Lipid-protein interactions mediate the photochemical function of rhodopsin. *Biochemistry.* 27:6469–6474.

68. Hong, H., and L. K. Tamm. 2004. Elastic coupling of integral membrane protein stability to lipid bilayer forces. *Proc. Natl. Acad. Sci. USA.* 101:4065–4070.

69. Bowie, J. U. 2005. Solving the membrane protein folding problem. *Nature* (*Lond.*). 438:581–589.

70. McMahon, H. T., and J. L. Gallop. 2005. Membrane curvature and mechanisms of dynamic cell membrane remodelling. *Nature (Lond.).* 438:590–596.

71. Booth, P. J. 2005. Same in the membrane: designing systems to modulate membrane proteins. *Curr. Opin. Struct. Biol.* 15:435–440.

72. Zimmerberg, J., and M. M. Kozlov. 2006. How proteins produce cellular membrane curvature. *Nat. Rev. Mol. Cell Biol.* 7:9–19.

73. Jensen, J. W., and J. S. Schutzbach. 1984. Activation of mannosyltransferase II by nonbilayer phospholipids. *Biochemistry.* 23:1115–1119.

74. Navarro, J., M. Toivio-Kinnucan, and E. Racker. 1984. Effect of lipid composition on the calcium/adenosine 5′-triphosphate coupling ratio of the Ca^{2+}-ATPase of sarcoplasmic reticulum. *Biochemistry.* 23: 130–135.

75. Lindblom, G., I. Brentel, M. Sjölund, G. Wikander, and Å. Wieslander. 1986. Phase equilibria of membrane lipids from *Acholeplasma laidlawii*. The importance of a single lipid forming nonlamellar phases. *Biochemistry.* 25:7502–7510.

76. Keller, S. L., S. M. Bezrukov, S. M. Gruner, M. W. Tate, I. Vodyanoy, and V. A. Parsegian. 1993. Probability of alamethicin conductance states varies with nonlamellar tendency of bilayer phospholipids. *Biophys. J.* 65:23–27.

77. Owicki, J. C., and H. M. McConnell. 1979. Theory of protein-lipid and protein-protein interactions in bilayer membranes. *Proc. Natl. Acad. Sci. USA.* 76:4750–4754.

78. Killian, J. A. 1998. Hydrophobic mismatch between proteins and lipids in membranes. *Biochim. Biophys. Acta.* 1376:401–416.

79. Watts, A., I. D. Volotovski, and D. Marsh. 1979. Rhodopsin-lipid associations in bovine rod outer segment membranes. Identification of immobilized lipid by spin-labels. *Biochemistry.* 18:5006–5013.

80. Sheikh, S. P., T. A. Zvyaga, O. Lichtarge, T. P. Sakmar, and H. R. Bourne. 1996. Rhodopsin activation blocked by metal-ion-binding sites linking transmembrane helices C and F. *Nature* (*Lond.*). 383: 347–350.

81. Vogel, R., J. Ruprecht, C. Villa, T. Mielke, G. F. X. Schertler, and F. Siebert. 2004. Rhodopsin photoproducts in 2D crystals. *J. Mol. Biol.* 338:597–609.

82. Szundi, I., J. J. Ruprecht, J. Epps, C. Villa, T. E. Swartz, J. W. Lewis, G. F. X. Schertler, and D. S. Kliger. 2006. Rhodopsin photointermediates in two-dimensional crystals at physiological temperatures. *Biochemistry.* 45:4974–4982.

83. Fotiadis, D., B. Jastrzebska, A. Philippsen, D. J. Müller, K. Palczewski, and A. Engel. 2006. Structure of the rhodopsin dimer: a working model for G-protein-coupled receptors. *Curr. Opin. Struct. Biol.* 16:252–259.

84. Nagle, J. F., and S. Tristram-Nagle. 2000. Structure of lipid bilayers. *Biochim. Biophys. Acta.* 1469:159–195.

85. Israelachvili, J. 1992. Intermolecular and Surface Forces, 2nd Ed. Academic Press, New York.

86. Salamon, Z., M. F. Brown, and G. Tollin. 1999. Plasmon resonance spectroscopy: probing molecular interactions within membranes. *Trends Biochem. Sci.* 24:213–219.

87. Gruner, S. M. 1989. Stability of lyotropic phases with curved interfaces. *J. Phys. Chem.* 93:7562–7570.

88. Seddon, J. M. 1990. Structure of the inverted hexagonal (H_{II}) phase, and non-lamellar phase transitions of lipids. *Biochim. Biophys. Acta.* 1031:1–69.

89. Olsson, U., and H. Wennerström. 1994. Globular and bicontinuous phases of nonionic surfactant films. *Adv. Colloid Interface Sci.* 49:113–146.

90. Lamola, A. A., T. Yamane, and A. Zipp. 1974. Effects of detergents and high pressures upon the metarhodopsin I-metarhodopsin II equilibrium. *Biochemistry.* 13:738–745.

91. Niu, S.-L., and D. C. Mitchell. 2005. Effect of packing density on rhodopsin stability and function in polyunsaturated membranes. *Biophys. J.* 89:1833–1840.

92. Salamon, Z., Y. Wang, J. L. Soulages, M. F. Brown, and G. Tollin. 1996. Surface plasmon resonance spectroscopy studies of membrane proteins: transducin binding and activation by rhodopsin monitored in thin membrane films. *Biophys. J.* 71:283–294.

93. Alves, I. D., G. F. J. Salgado, Z. Salamon, M. F. Brown, G. Tollin, and V. J. Hruby. 2005. Phosphatidylethanolamine enhances rhodopsin photoactivation and transducin binding in a solid supported lipid bilayer as determined using plasmon-waveguide resonance spectroscopy. *Biophys. J.* 88:198–210.

94. Cooper, A. 1979. Energy uptake in the first step of visual excitation. *Nature* (*Lond.*). 282:531–533.

95. Schick, G. A., T. M. Cooper, R. A. Holloway, L. P. Murray, and R. R. Birge. 1987. Energy storage in the primary photochemical events of rhodopsin and isorhodopsin. *Biochemistry.* 26:2556–2562.

96. Miljanich, G. P., M. F. Brown, S. Mabrey-Gaud, E. A. Dratz, and J. M. Sturtevant. 1985. Thermotropic behavior of retinal rod membranes and dispersions of extracted phospholipids. *J. Membr. Biol.* 85:79–86.

97. Sapra, K. T., P. S.-H. Park, S. Filipek, A. Engel, D. J. Müller, and K. Palczewski. 2006. Detecting molecular interactions that stabilize native bovine rhodopsin. *J. Mol. Biol.* 358:255–269.

98. van den Brink-van der Laan, E., J. A. Killian, and B. de Kruijff. 2004. Nonbilayer lipids affect peripheral and integral membrane proteins via changes in the lateral pressure profile. *Biochim. Biophys. Acta.* 1666:275–288.

99. Liang, Y., D. Fotiadis, S. Filipek, D. A. Saperstein, K. Palczewski, and A. Engel. 2003. Organization of the G protein-coupled receptors rhodopsin and opsin in native membranes. *J. Biol. Chem.* 278:21655–21662.

100. Park, P. S.-H., and K. Palczewski. 2005. Diversifying the repertoire of G protein-coupled receptors through oligomerization. *Proc. Natl. Acad. Sci. USA.* 102:8793–8794.

101. Chabre, M., R. Cone, and H. Saibil. 2003. Is rhodopsin dimeric in native retinal rods? *Nature* (*Lond.*). 426:30–31.

102. Fotiadis, D., Y. Liang, S. Filipek, D. A. Saperstein, A. Engel, and K. Palczewski. 2004. The G protein-coupled receptor rhodopsin in the native membrane. *FEBS Lett.* 564:281–288.

103. Jastrzebska, B., D. Fotiadis, G.-F. Jang, R. E. Stenkamp, A. Engel, and K. Palczewski. 2006. Functional and structural characterization of rhodopsin oligomers. *J. Biol. Chem.* 281:11917–11922.